CHEMISTRY OF MATERIALS

Article

pubs.acs.org/cm

Self-Assembly of Smart Multifunctional Hybrid Compartments with Programmable Bioactivity

Gong Cheng,[†,‡] Si-Jie Hao,[†] Yuan Wan,[†] Ding-Ying Shan,[†] Jian Yang,[†] and Si-Yang Zheng*[,†,‡]

[†]Department of Biomedical Engineering and [‡]Material Research Institute, The Pennsylvania State University, University Park, Pennsylvania 16802, United States

Supporting Information

ABSTRACT: Artificial microcompartments are highly desirable for understanding the mechanism of formation of primitive cells for the origin of life and have technological effects in broad fields such as materials science, catalysis, environmental remediation, biomedicine, and biotechnology. However, it remains a critical challenge for the construction of a structurally stable, semipermeable, and multifunctional compartment that can maintain a protective and confined internal space while allowing internalization of ingredients. Here, we present a strategy for construction of novel smart multifunctional hybrid compartments (SMHCs) with semipermeability, stimulus-response, and enzymatic bioactivity. The smart compartments were assembled by packing magnetic nanoparticles on oil/water interface, and the interstitial pores were gated by designed thermosensitive copolymer brushes. The materials characterization, multifunctionality, and on-demand permeability of prepared hybrid compartments were investigated. Notably, biological macromolecules can be easily encapsulated without sacrifice of the original bioactivity. We exploited the reversible permeability of these responsive inorganic−organic smart compartments, demonstrated temperature-triggered release of small molecules, and displayed SMHCs as a light programmable artificial microreactor.

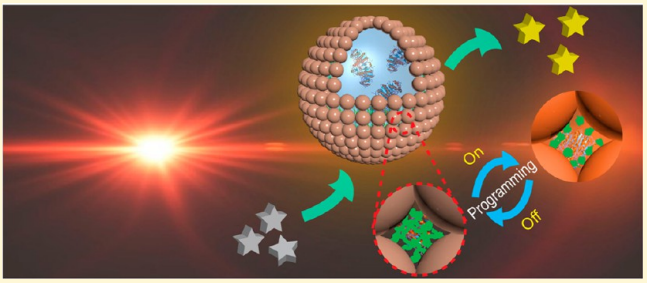

INTRODUCTION

As one the of basic building units of life, the cell is a compartmentalized space with an outer membrane and multiple internal organelles, which can mediate many complex biochemical reactions in concert and provide specialized cellular functions.[1] By mimicking biological compartmentalization, the design and construction of the smart artificial compartments based on bottom-up strategies attract particular attention in various fields.[2−6] A typical artificial compartment has a lumen segregated from the external environment by a membrane, while accessible and tunable pores on the membrane would allow small molecules to pass through. The encapsulate cargo thus can be effectively protected against potential damage and controllably released. This property is particularly important in the fields of biomedicine and catalysis involving bioactive protein cargos.[7−10] For instance, the smart compartments either as bioreactors or as delivery vehicles are expected to shelter protein cargos from attack of protease.[11,12] To date, various approaches have been explored to artificial compartments.[13−17] Among them, use of a template to create "hollow cavity" is the most common technique.[18−21] However, one of the major challenges is the incorporation of guest biomolecules while maintaining their bioactivity. Moreover, existing artificial compartments show a sole response to pH or ionic strength for on-demand permeability.[22,23] They are still not effective to accomplish a variety of advanced applications and show inferior potency in comparison with multistimuli responsive ones. Hence, smart multifunctional compartments with intact structure and semipermeable membrane for facile encapsulation of bioactive molecules are highly desirable.

With development of nanotechnology, self-assembly of nanoscale materials to form hierarchically ordered structures provides new chances to construct functional compartments.[24−30] Especially, Pickering emulsions stabilized by a wide range of colloidal particles can easily and directly encapsulate molecules into compartment during emulsification.[31,32] Although promising, the inherent stability arising from the noncovalent interactions between particle/particle/liquids is not strong enough to keep the intact structure in pure aqueous solution. In addition, small molecules can rapidly diffuse out through the interstitial pores on the membrane assembled by nanoparticles. To address these concerns, both the development of new nanoblocks and the design of membrane with on-demand permeability are important. Herein, we report the design and preparation of novel smart multifunctional hybrid compartments (SMHCs), which can compatibly encapsulate guest biomacromolecules for programmable biofunction (Scheme 1). SMHCs are constructed by self-assembly of partially hydrophobic magnetic nanoparticles on the oil/water interface of the emulsions and simultaneously

Received: October 10, 2016
Revised: February 15, 2017
Published: February 15, 2017

DOI: 10.1021/acs.chemmater.6b04326
Chem. Mater. 2017, 29, 2081−2089

Scheme 1. (a) Construction of SMHCs by Self-Assembly of Magnetic Nanoparticles on Water-in-Oil Droplets; (b) Reversible on/off of Stimulus-Responsive Gate of SMHCs by Either Temperature or NIR Light for Programmable Reaction

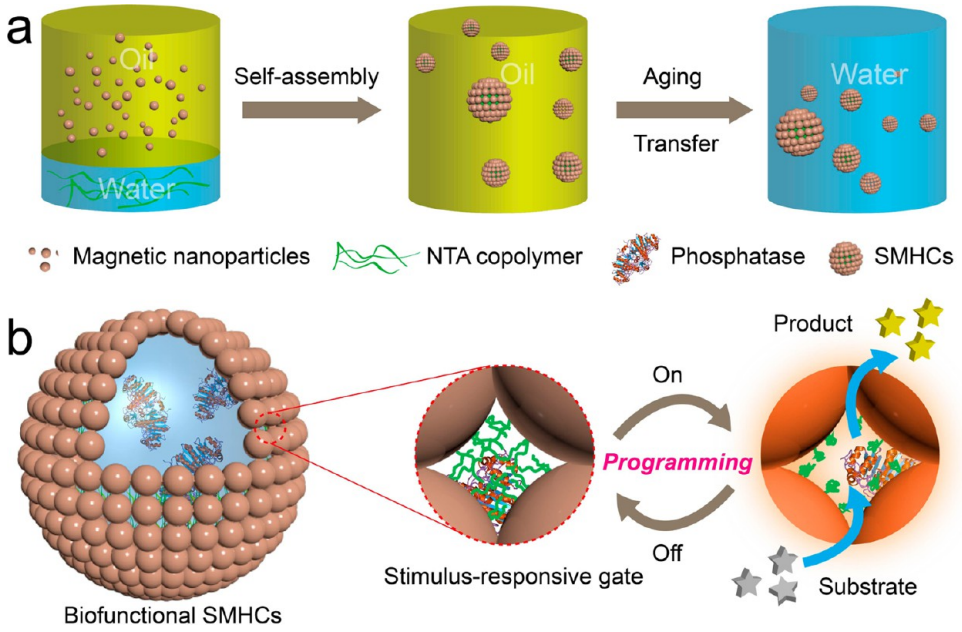

cross-linked by a designed smart thermosensitive copolymer brushes to gate the formed interstitial nanopores. Importantly, the self-assembly at oil/water interfaces allows us to encapsulate almost any guest molecules with high capacity at ease. Moreover, the multifunctional inorganic−organic hybrid membrane with mild photothermal responsibility can induce the conformational change of smart polymer brushes to open or close the gated nanopores and thus enable the reversible membrane permeability to be controlled by both temperature and near-infrared (NIR) light. Selective and dynamic permeability and the stimulus-response mechanism of the multifunctional hybrid colloidosome compartments have been investigated. We finally demonstrate that programmable dephosphorylation reaction can be achieved by confining phosphatases in the smart multifunctional hybrid compartments.

EXPERIMENTAL SECTION

Materials. Ferric chloride ($FeCl_3·6H_2O$), tris(hydroxymethyl)-aminomethane (Tris), hydrogen chloride (HCl), fluorescein (FITC), sodium acetate (NaAC), ethylene glycol, trisodium citrate, toluene, ethanol, sodium acetate, ethanol, dichloromethane, diethyl ether, and acetone were obtained from Alfa Aesar. Tetraethyl orthosilicate (TEOS), *N*-isopropylacrylamide (NIPAA), 3-(trimethoxysilyl)propyl methacrylate (TPM), acrylamide (AA), azobis(isobutyronitrile) (AIBN, recrystallized), tetramethoxysilane (TMS), octyltriethoxysilane (OTS), Rhodamine 6G (Rh6G), alkaline phosphatase (ALP), 4-nitrophenyl phosphate (NPP), methanol, and dodecane were purchased from Sigma-Aldrich. All chemicals and reagents were used directly without further purification.

Synthesis and Modification of Core−Shell Magnetic Nanoparticles. Carboxyl Fe_3O_4 nanoparticles with excellent dispersibility were prepared by a solvothermal method.[33] Typically, 2.16 g of $FeCl_3·6H_2O$ and 0.40 g of trisodium citrate were dissolved in 40 mL of ethylene glycol under vigorous stirring, and then 2.40 g of NaAc was added. The mixture was stirred for 30 min and followed by ultrasonication for another 30 min. Then the mixture was transferred to a Teflon-lined stainless-steel autoclave and heated at 200 °C for 12 h. The black product was collected and washed with ethanol and deionized water for several times and, finally, vacuum-dried at 60 °C.

Then silica was coated onto the Fe_3O_4 nanoparticles by a modified Stöber method to form magnetic silica (MS).[34] Briefly, 60 mg of as-prepared Fe_3O_4 nanoparticles was ultrasonically dispersed in a solution containing 300 mL of ethanol, 60 mL of water, and 6 mL of concentrated ammonia (28 wt %). Then 0.4 mL TEOS was added dropwise to the solution under ultrasonication followed mechanical stirring for 10 h at room temperature. Subsequently, the particles were collected and washed with deionized water and ethanol for several times before drying at 60 °C for 12 h.

Surface modification of as prepared core−shell magnetic nanoparticles was conducted to optimize their wettability. A predetermined amount of OTS and 300 mg of MS nanoparticles were dispersed in 20 mL of toluene under ultrasonication for 30 min. The mixture was then transferred to a Teflon-lined stainless-steel autoclave and heated at 120 °C for 12 h. The product (MS-OTS) was collected and washed with toluene and ethanol for several times before drying at 60 °C for 12 h.

Synthesis and Characterization of Thermosensitive Copolymer Brushes. Copolymer brushes (poly NIPAA-AA-TPM; NAT) were synthesized by free radical copolymerization. Briefly, NIPAA, TPM, AA, and AIBN in designed molar ratios were dissolved in methanol and degassed by the nitrogen purge for half an hour. The solution was stirred and heated at 65 °C under the nitrogen atmosphere for 24 h. Residual methanol in the resulted mixture was evaporated. The product was dissolved in dichloromethane and then precipitated out by adding the diethyl ether. This step was repeated several times to purify the product. The final copolymer brushes were dried under vacuum and stored in a desiccator before use. The lower critical solution temperature (LCST) was determined by plotting the temperature of cloud point. The absorption of the copolymer at 450 nm was continuously measured against temperature at a heating rate of 1.0 °C min^{-1} using a multimode reader equipped with a temperature controller.

Construction of SMHCs. Nanoparticle-stabilized water-in-oil Pickering emulsions were first prepared. Typically, core−shell magnetic nanoparticles were well dispersed in oil (dodecane) with a concentration of 10 mg mL^{-1} by ultrasonication, while the NAT copolymer brushes were dissolved in deionized water at a concentration of 1 mg mL^{-1}. Three-hundred microliters of the above nanoparticles dispersion was added to 100 μL of NAT aqueous solution with Rh6G fluorescent dye or bioactive phosphatase. The water-in-oil Pickering emulsions were formed by vigorously shaking with a vortex shaker for 2 min. Afterward, additional 0.5 mL of oil was

DOI: 10.1021/acs.chemmater.6b04326
Chem. Mater. 2017, 29, 2081−2089

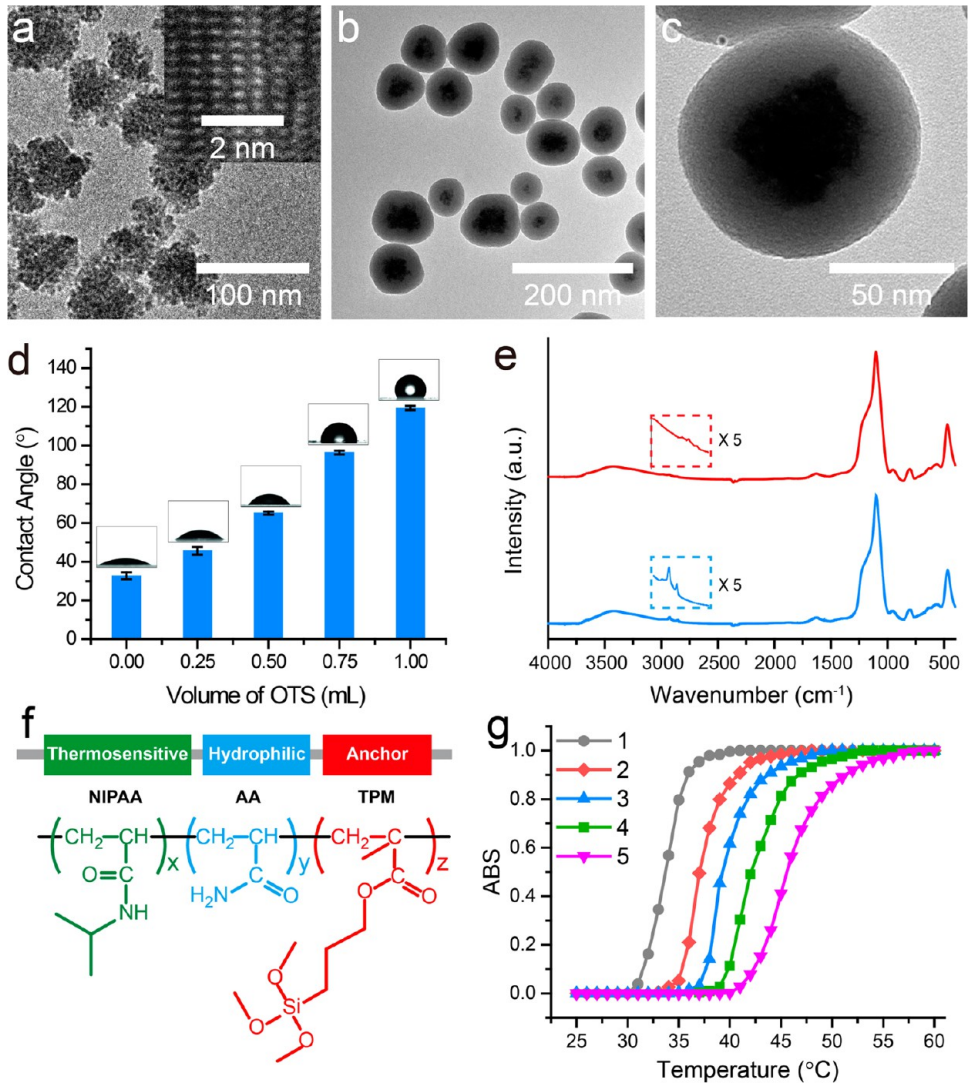

Figure 1. (a) TEM and HRTEM (inset) images of the Fe_3O_4 nanoparticles. (b, c) TEM images of the synthesized MS nanoparticles. (d) The contact angle of MS modified with different amount of OTS. (e) FTIR spectra of MS (red) and MS-OTS (blue). (f) Chemical structure of the designed copolymer brush (NAT) with functional monomers. Note: different monomers were randomly distributed in the NAT copolymers, and the sketch only represents the accurate chemical structure of the monomers included in the copolymers. (g) The LCST temperature of the polymer brush was tuned by hydrophilic monomers with different NIPAA/AA/TPM ratios: (1) 100/0/2, (2) 97.5/2.5/2, (3) 95/5/2, (4) 92.5/7.5/2, (5) 90/10/2.

added, and the nanoparticles-stabilized emulsions stood still for 1 h in a refrigerator (4 °C). Then 30 μL of TMS was added to the Pickering emulsions, and the dispersion was rotated gently for 5 min before standing still. After 6 h, 30 μL of TMS was added, and the mixture aged overnight with gentle mixing occasionally. To transfer the prepared SMHCs from oil phase to aqueous phase, 200 μL of acetone was added to above mixture, and the mixture stood for 30 min. The supernatant oil was removed, and SMHCs were washed with acetone and water to remove possible broken fragments and unencapsulated or leaked fluorescent dye or ALP enzyme before redispersed in 1 mL of aqueous solution. To determine the amount of encapsulated fluorescent dye, the final SMHCs were dispersed in 0.5 mL of ethanol and followed by ultrasonication for 2 h. After rotation and vibration for 24 h, the solution with dye was recovered, and the residuals were dissolved in aqueous solution after evaporation of ethanol.

Permeability and Stability Characterization of SMHCs. The controllable permeability of prepared SMHCs was evaluated by the on-demand release of Rh6G encapsulated in the SMHCs. Rh6G solution (100 μg mL^{-1}) was encapsulated in the SMHCs during the formation of Pickering emulsions. The final SMHCs (3 mg mL^{-1}) were redispersed in 10 mL of aqueous solution at different temperatures (37 and 40 °C). The time-dependent concentrations of released Rh6G in the continuous phase of water were determined by recording the fluorescence intensities using a fluorescence spectrometer. The optical and fluorescent microscopy images of typical SMHCs before and after the release of the dye were also observed using a fluorescent microscope. To avoid the possible deviation arising from the size of SMHCs or the photobleaching of dye during exposure to the light excitation source, SMHCs with the same size were snapshotted under the same exposure condition rapidly. To check the permeability of prepared SMHCs for ALP molecules, the FITC-labeled ALP was caged in SMHCs as described above. Then SMHCs (3 mg mL^{-1}) were redispersed in 10 mL of aqueous solution at different temperatures (37 and 40 °C). The optical and fluorescence microscopy images of typical SMHCs before and after the release of the dye were recorded using fluorescence microscopy. For evaluation of the stability, SMHCs (3 mg mL^{-1}) were incubated at 37 °C (below the LCST) and 40 °C (above the LCST) for 3 days, respectively. The resultant SMHCs were collected by a magnet, and the aqueous phase was evaporated at room temperature. The morphology of the SMHCs before and after incubation was observed using the SEM equipment.

DOI: 10.1021/acs.chemmater.6b04326
Chem. Mater. 2017, 29, 2081−2089

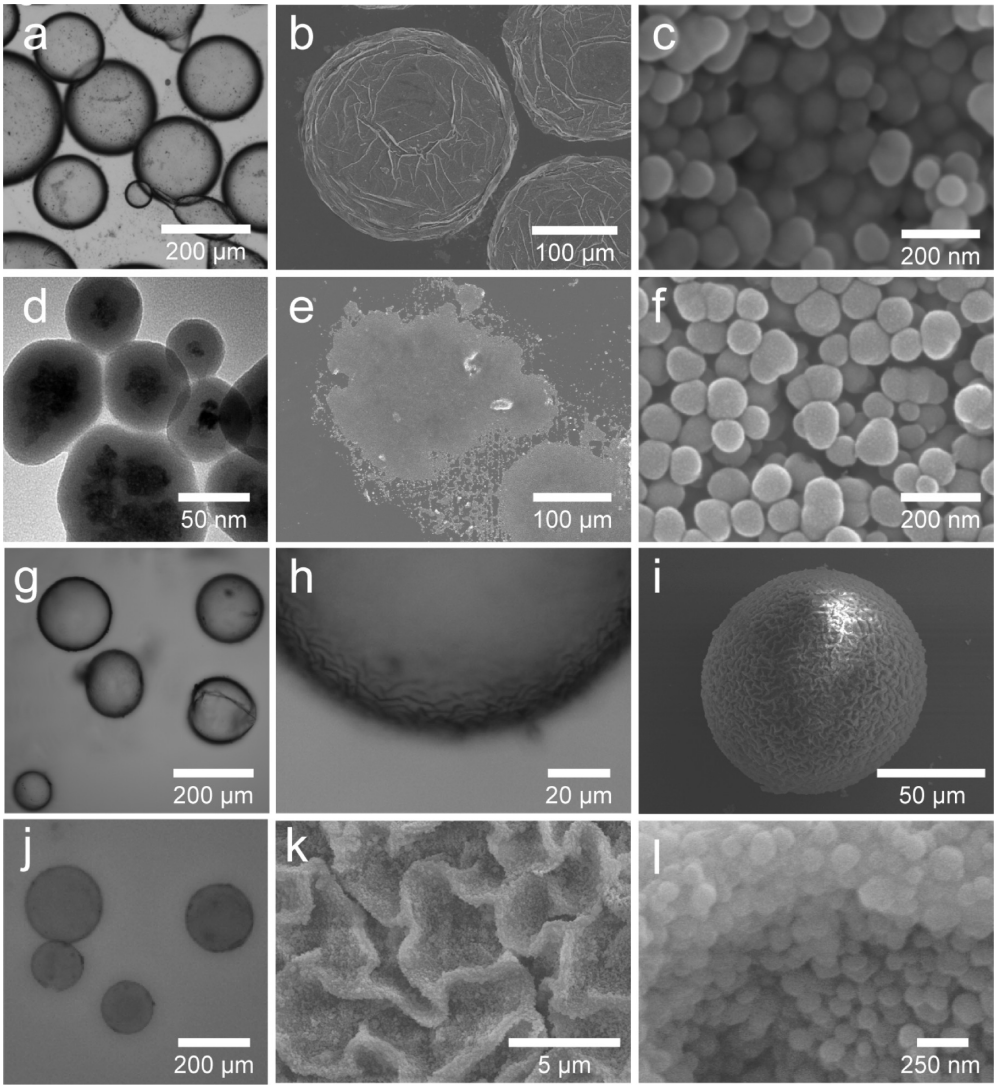

Figure 2. (a) Microscopy, (b, c) SEM, and (d) TEM images of magnetic nanoparticles assembled capsules with NAT copolymer brushes. (e, f) SEM images of collapsed compartments due to the absence of NAT copolymer. (g, h) Microscopy images of SMHCs in oil and (j) aqueous solution. (i, k, l) SEM images of a free-standing SMHC.

Biofunctional SMHCs for Programming Dephosphorylation. Biofunctional SMHCs (100 μL, 3 mg mL^{-1}) caged with 0.1 U ALP enzymes were added into 2 mL of 25 μM NPP solution (dissolved in Tris-HCl buffer containing 1 mM $MgCl_2$, pH = 9.5) at the different temperatures (37 and 40 °C) to mediate the dephosphorylation. Dephosphorylated product 4-nitrophenolate (NP) in the continuous aqueous phase was monitored over time at 410 nm by a UV−vis spectrometer. Control experiments of enzymatic dephosphorylation using pure ALP were also conducted at the predetermined temperatures.

NIR-induced dephosphorylation by stimulus-responsive SMHCs was remotely controlled using a continuous wave (CW) diode laser (DS3−11322−110-K808/980F14CD, BWT Beijing Ltd., China) with the wavelength of 808/980 nm. The irradiation area of the laser was a circular spot with the diameter of 1 cm. The irradiation position was accurately aligned and focused on the SMHCs with the help of the equipped visible light beam. The power density was first optimized by tuning the laser power, and the laser power density of 3.18 W cm^{-2} was used for following experiments. To investigate the thermal reversibility, SMHCs (0.15 mg mL^{-1}) were incubated with 2 mL of 25 μM NPP solution (dissolved in Tris-HCl buffer containing 1 mM $MgCl_2$, pH = 9.5), and the dephosphorylation mediated by the biofunctional SMHCs were repeatedly regulated 10 times with the 20 min laser on and 60 min laser off for each cycle, while the dephosphorylated product NP in the continuous aqueous phase was monitored after each step at 410 nm by a UV−vis spectrometer (Infinite 200 PRO).

Characterizations. Scanning electronic microscopy (SEM) images were obtained on a field emission scanning electron microscope (FESEM; NanoSEM 630, NOVA), equipped with an energy-dispersive X-ray analysis (EDXA) system. Transmission electron microscopy (TEM) images were taken with a JEOL-2010 microscope at the accelerating voltage of 200 kV. X-ray diffraction (XRD) patterns were collected on a PANanlytical Empyrean X-ray powder diffractometer. UV−vis−NIR spectra were recorded on a PerkinElmer Lambda 950 UV−vis−NIR spectrophotometer. Samples for NMR spectroscopy were recorded in $CDCl_3$ using a Bruker 400 Ultrashield spectrometer operating at 400 MHz. Fourier transform infrared (FTIR) spectra were determined on a Bruker Vertex V70 FTIR spectrometer and scanned from 400−4000 cm^{-1} at a resolution of 6 cm^{-1}. Water contact angles were measured with a contact angle goniometer (rame-hart model 260 Automated Goniometer/Tensiometer) by the sessile water drop method with 5 μL water drops. Magnetization measurements of the core−shell magnetic nanoparticles and SMHCs were carried out with a superconducting quantum interface device (SQUID) magnetometer at 300 K. Fluorescence intensity and spectra were recorded on a HORIBA Scientific Fluoromax-4 spectrofluorometer. The absorbance of NP at 410 nm was determined on an Infinite 200 PRO multimode

DOI: 10.1021/acs.chemmater.6b04326
Chem. Mater. 2017, 29, 2081−2089

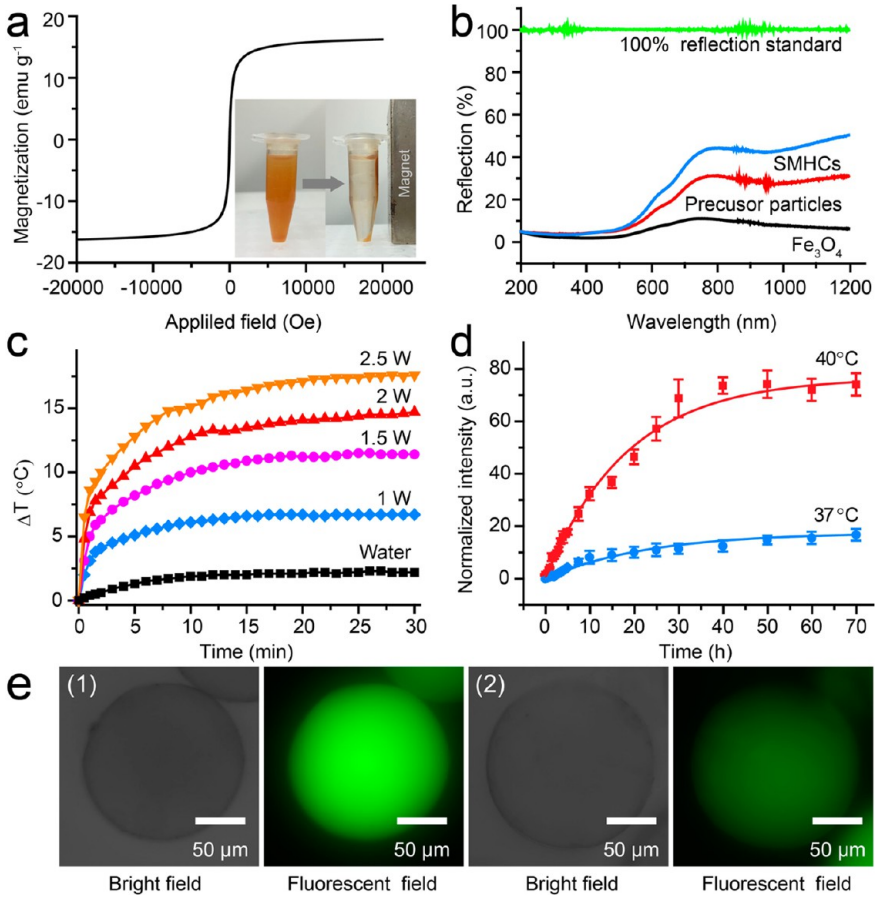

Figure 3. (a) Magnetic hysteresis loops of the SMHCs, and (inset) the magnetic manipulation of SMHCs with the external magnetic field. (b) UV−vis−NIR diffused reflection spectra of prepared Fe_3O_4 nanoparticles, precursor nanoparticles, and the SMHCs. (c) Photothermal effect of the SMHCs under laser irradiation with different power. (d) Release of the fluorescence dye from SMHCs at different temperatures. (e) Fluorescence microscopy images of SMHCs with encapsulated dye: (1) before release, (2) after release at 40 °C for 70 h.

UV−vis reader. Microscopy images were obtained on a fluorescence microscope (Leica). Confocal fluorescence microscope (Olympus FV1000 laser scanning confocal microscope) with automatic Z-scanning was used to further study the enzyme distribution inside the artificial cells. The thermal images of SMHCs under NIR radiation were taken by an infrared thermometer (Fluke, USA) at designated time intervals.

RESULTS AND DISCUSSION

Preparation of Magnetic Nanoparticles and NAT Polymers. First, Fe_3O_4 nanoparticles (diameter: ~60 nm) with excellent dispersibility as building blocks of SMHCs were synthesized (Figures 1a and S1). High-resolution TEM (HRTEM) image (Figure 1a, inset) and X-ray diffraction pattern of Fe_3O_4 (Figure S1d) indicate these magnetic nanoparticles correlate well with cubic magnetite (JCPDS No. 19−0629).[35] Fe_3O_4 nanoparticles were further coated with a silica shell (MS, Figure 1b,c). The stability of nanoparticles on the oil/water interface depends on surface wettability, which can be visualized by contact angle (Figure 1d). Nanoparticles with a contact angle of 90° have optimum stability at the oil/water interface as they require the lowest transfer energy (Figure S2).[36] Therefore, we prepared magnetic colloids with the contact angle of 95.4° (Figure 1d) through optimizing the density of grafted alkyl residues of OTS. The presence of vibration bands at 2856 cm^{-1} and 2925 cm^{-1} ($-CH_3$, $-CH_2$) in FTIR spectrum of OTS-modified MS confirms the successful surface modification (Figure 1e). We also designed a smart thermosensitive copolymer brush composing of active anchors and temperature sensitive units as the thermosensitive molecular gate of SMHCs. The copolymer brush NAT (Figure 1f) includes thermal responsive monomer (*N*-isopropylacrylamide; NIPAA), hydrophilic adjuster (AA), and active anchor (TPM). The composition of NAT copolymers was verified by NMR and FTIR spectra (Figure S3a,b). The NAT copolymer can conformationally switch from expanded coil to compact globule at LCST,[37−39] and the LCST can be tuned by copolymerization of different proportion of AA hydrophilic monomers (Figure 1g). To accommodate to most of the biomolecules, we chose the thermal responsive window of 38−42 °C. As shown in Figure S3c, NAT is responsive to temperature, and reversible phase transitions of the NAT copolymer can be realized.

Construction and Characterization of SMHCs. To construct SMHCs, aqueous solution with NAT copolymer was introduced into oil phase containing nanoparticles, followed by shaking to generate emulsions (Figure S4). Then nanoparticles assembled capsules were formed (Figure 2a), which present polydispersity in size. Interestingly, after evaporation of the solvent, intact but deflated balloon-like capsules were observed (Figure 2b). NAT copolymer brushes play a pivotal role in the formation of intact capsules, as they can further cross-link the self-assembled nanoparticles (Figure 2c,d). Notably, the reactive silane coupling groups in NAT

DOI: 10.1021/acs.chemmater.6b04326
Chem. Mater. 2017, 29, 2081−2089

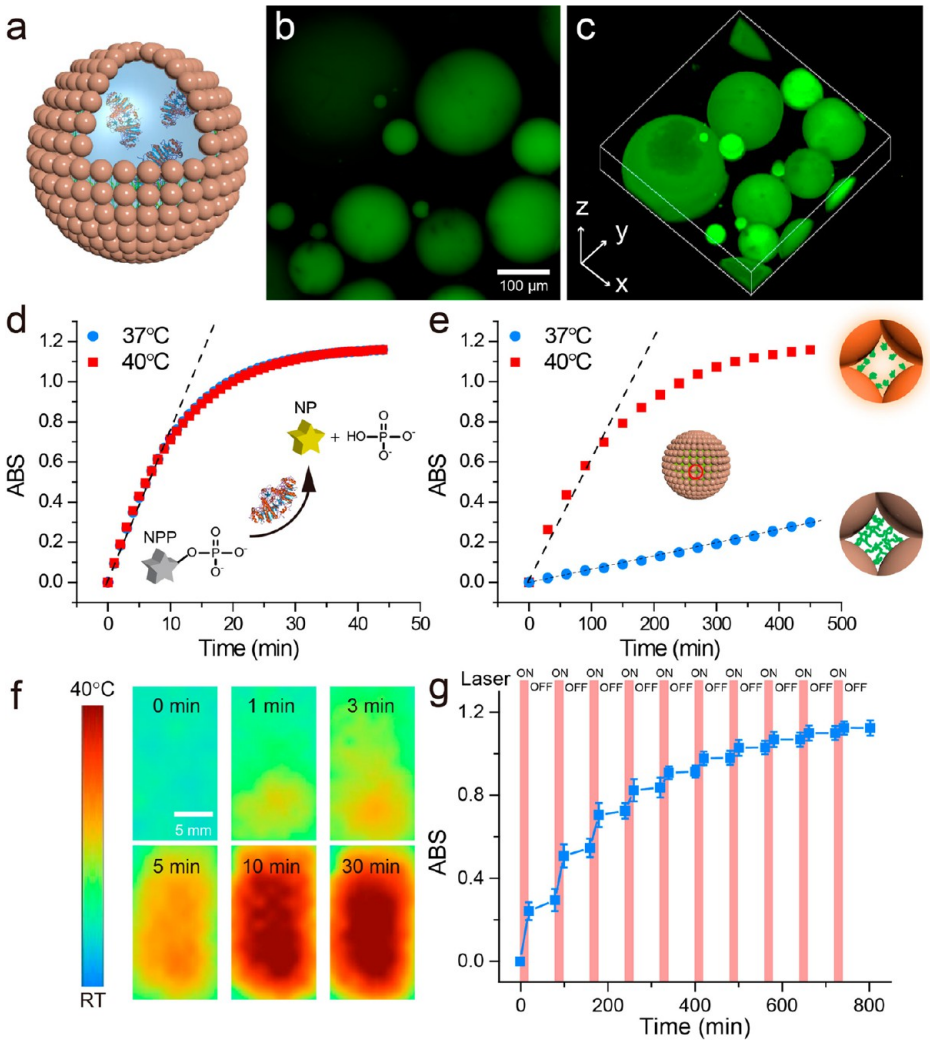

Figure 4. (a) Illustration of SMHCs artificial microreactor. (b) 2D and (c) 3D confocal fluorescence microscopy of SMHCs with caged phosphatases. (d) Time-dependent changes of the dephosphorylation induced by free phosphatases and (e) the artificial microreactors in the continuous aqueous phase at different temperatures. (f) Thermographic images of the SMHCs suspension recorded under NIR irradiation at the different time. (g) Programming SMHCs induced dephosphorylation by NIR light with several on/off cycles.

copolymers would covalently react with the hydroxy groups on the silica surface, which would result in the covalent cross-link of the adjacent magnetic silica nanoparticles (Figure S5). In contrast, without NAT polymer cross-linking nanoparticles, the assembled microcompartments dissembled after solvent evaporation (Figure 2e), and only residual randomly dispersed nanoparticles could be observed (Figures 2f and S6). After further aging, the NAT cross-linked capsules, intact and stable SMHCs were prepared (Figure 2g). Interestingly, SMHCs have the typical wrinkled surface (Figure 2h). These SMHCs can be easily transferred into the pure aqueous phase with intact structure (Figure 2j). Evaporation of solvent would result in the significant shrinkage of SMHCs (Figure S7), indicating their inherent flexibility and elasticity. According to SEM characterization, the free-standing and intact SMHCs with spherical morphology can be observed (Figure 2i). Apparently, SMHCs are assembled by nanoparticles (Figure 2k,l), and these nanoparticles are cross-linked and gated by NAT copolymer (Figure S8a,b), which is also evidenced by the presence of characteristic absorption bands of NAT in the FTIR spectrum of the SMHCs (Figure S8c). The intrinsic nature of SMHCs was confirmed by X-ray diffraction analysis, and they have the same crystalline phases as the precursor magnetic nanoparticles (Figure S9).

Multifunctionality and Dynamic Permeability of SMHCs. After basic characterization of SMHCs, we studied their multifunctionality and stability. As core−shell magnetic silica nanoparticles were used as building blocks, SMHCs have superparamagnetism at room temperature with the saturation magnetization (M_s) value of 16.2 emu g^{-1} (Figure 3a), and thus, they can be freely manipulated by an external magnetic field (Figure 3a, inset). Moreover, SMHCs also have NIR light responsiveness, and they have a relatively strong absorbance in the NIR range (Figure 3b), owing to the NIR absorbance of Fe_3O_4 building nanoblocks.[40] Under NIR light radiation, Fe_3O_4 nanoparticles building blocks can mildly respond to NIR light and convert optical energy to local heating. Thus, the temperature of the SMHCs increased rapidly and then stabilized at a certain temperature depending on the laser power (Figure 3c). The long-term stability of SMHCs below or above the LCST was then investigated. As revealed in Figure S10, even after incubation at the temperature above the LCST for over 3 days, SMHCs keep the spherical structure, and their morphology is almost the same as that before incubation. The

DOI: 10.1021/acs.chemmater.6b04326
Chem. Mater. 2017, 29, 2081−2089

stability of SMHCs could be ascribed to the covalent cross-link of self-assembled magnetic silica nanoparticles by multifunctional NAT copolymers and TMS agents.

Then we further evaluated the dynamic permeability of SMHCs by the release of encapsulated fluorescence dye Rh6G (Figure S11). The fluorescence dye molecules were easily encapsulated in SMHCs during formation of emulsion droplets. Then the SMHCs with dye-containing liquid core were transferred into the aqueous solution. At different temperatures, the fluorescence intensities of aqueous solutions with released dye molecules were recorded periodically. It should be noted that the slight increase in temperature from 37 to 40 °C would not significantly influence the dye diffusion.[41] As shown in Figure 3d, the increased fluorescence intensity of aqueous solutions revealed that initially encapsulated dye could rapidly diffuse out from SMHCs at the temperature above the LCST, as molecule gate of NAT copolymer brushes was open. However, the diffusion is much slower at the temperature below the LCST due to the closed NAT gate. Furthermore, after release for 70 h, fluorescence microscopy images (Figure 3e) show that the fluorescence intensity of individual SMHCs in water significantly decreased at the temperature above the LCST in comparison of that at the low temperature (Figure S12), due to the release of the dye molecules. These results demonstrate that SMHCs have temperature-dependent controllable permeability.

Biofunctional SMHCs as Artificial Microreactors for Programmable Biocatalysis. Phosphorylation/dephosphorylation, one of the most common while significant post-translational modifications, regulates various cellular processes such as metabolism, signaling, cell growth, and division.[42] Inspired by the multifunctionality and on-demand permeability of SMHCs, we demonstrated that alkaline phosphatase (ALP) embedded SMHCs can be used as an artificial microreactor for performing in situ dephosphorylation (Figure 4a). This biomimicking model system we developed would be helpful in understanding the signaling pathways in protocell.[43] Phosphatases were caged in SMHCs directly during the formation of the water-in-oil emulsions, and SMHCs could be transferred into the aqueous solution. The encapsulation of fluorescence-labeled ALP molecules was confirmed under 2D/3D confocal fluorescence microscopy first (Figure 4b,c). The Z-optical axis confocal imaging revealed caged ALP molecules evenly distribute in the core (Figure S13). As shown in Figure S14, these ALP molecules were well caged in with no apparent leakage even the temperature increased to above LCST. It is due to the relatively large size of ALP molecules (~6.2−8.3 nm) compared with the interstitial pore size of the SMHCs.[44] Importantly, the nanopores on the semipermeable hybrid membrane were gated by thermal sensitive NAT polymer brushes. Thus, the bioactivity of caged phosphatases can be controlled by the thermal stimulus to regulate the accessibility of the substrate and product molecules diffusion between the outside continuous aqueous phase and confined compartment. As an example, we tested their controllable dephosphorylation of a colorless substrate, 4-nitrophenyl phosphate (NPP). The formation of dephosphorylated product, the yellow 4-nitrophenolate (NP), was monitored by measuring the optical absorption at 410 nm (Figure S15). As shown in Figure 4d, when the temperature of SMHCs was moderately elevated to 40 °C, the polymer brushes gated nanopores were opened. Thus, the colorless substrates NPP were able to enter into the liquid core of SMHCs through opened pores. Once NPP meets ALP, it is dephosphorylated and thus rapidly converted to NP, which resulted in the strong absorbance. In comparison, at 37 °C below the LCST, the entrance was blocked, and thus few NPP could cross the membrane, which resulted much slower color change (Figure 4e). As a result, the dephosphorylation rate at 40 °C was approximately eight-fold faster than that at 37 °C. However, for dephosphorylation induced by pure phosphatase, the dephosphorylation rate was almost the same in pure phosphatase solution at 37 and 40 °C, respectively (Figure 4d). Therefore, the dephosphorylation rate in SMHCs was controlled by the temperature stimulus responsive permeability of the hybrid membrane.

More importantly, SMHCs have the NIR responsibility, as we demonstrated above. NIR light is relatively moderate to biomolecules and even biological tissues.[45] This inspired us to remotely program the functionality of biomolecules by NIR light stimulus-responsive SMHCs. Intrinsically, under NIR radiation, Fe_3O_4 nanoparticles in SMHCs mildly convert optical energy to local heating (Figure 4f), while the extreme fever to impair the biomolecules is avoided.[46] When the temperature of the artificial compartments is above/below the LCST, the copolymer gated nanopores are triggered to be open/close remotely. The dynamic permeability of the SMHCs would lead to the programmed functionality of confined phosphatase. As shown in Figure 4g, the biofunctional SMHCs were irradiated by a NIR laser for several cycles of the laser on/off. When the laser was on, the dephosphorylation started upon irradiation. However, when the laser was off, the reaction slowed down significantly. The dephosphorylation can be easily programmed by switching the laser on/off for many cycles, manifesting the SMHCs can be used as light-remoted artificial microreactors for programmable dephosphorylation reaction.

The above results have shown the construction of novel stimulus-responsive artificial compartments by confining biomolecules in multifunctional inorganic−organic hybrid colloidosome capsules. In comparison with traditional capsules prepared by template-based strategy, the SMHCs offer an easy and biocompatible approach for loading the guest molecules. The SMHCs were assembled by magnetic nanoparticles packing on water-in-oil droplet, while these nanoparticles were cross-linked by the NAT smart copolymer brushes. The inherent elasticity and rigidness arising from the inorganic−organic hybrid structure enable the free-standing and intact structure of SMHCs, and they can be stable in pure aqueous solution, which differentiates them from other reported emulsion microcompartments. Although a few monofunctionally responsive (pH sensitive) smart compartments have been reported, they are limited to only pH-resistant biomolecules, and application of these compartments is also compromised by their monofunction. Slight fluctuation of temperature has negligible effects on most of the biomolecules, and SMHCs have temperature-sensitive and controllable permeability, in virtue of their NAT temperature-responsive polymer gated mesoporous shell. More importantly, the multifunctionality of SMHCs provides multiple approaches (temperature and remote NIR light) for manipulating their shell permeability. These could offer substantial advantages in the construction and application of the biomimetic system.

■ CONCLUSION

In conclusion, novel SMHCs have been developed by self-assembly of magnetic nanoparticles in Pickering emulsions and further cross-link with designed thermosensitive copolymer

DOI: 10.1021/acs.chemmater.6b04326
Chem. Mater. 2017, 29, 2081−2089

brushes. Our SMHCs can be easily transferred from oil to aqueous solution without destroying their intact structure. By using multifunctional magnetic nanoparticles as the hybrid building blocks, the SMHCs have excellent magnetism and mild NIR photothermal response. Moreover, SMHCs have the dynamic and selective permeability at water/water phase boundaries, enabling protection of encapsulated cargo or temperature/light stimulus responsive release of cargo molecules. Furthermore, SMHCs were explored as microbioreactors by performing programmed dephosphorylation in the core. Therefore, our work provides a new solution for the construction of biomimetic systems for regulating bioactivity of biomolecules, and the SMHCs can also be used as bioreactors, biosensors, and drug delivery vehicles in various research fields.

■ ASSOCIATED CONTENT

Supporting Information

The Supporting Information is available free of charge on the ACS Publications website at DOI: 10.1021/acs.chemmater.6b04326.

Characterization of responsive copolymer brushes, magnetic nanoparticles, and colloidosome microcapsules; detailed study and discussion of stability and controllable permeability of SMHCs (PDF)

■ AUTHOR INFORMATION

Corresponding Author

*E-mail: sxz10@psu.edu.

ORCID

Gong Cheng: 0000-0002-2217-6408
Si-Yang Zheng: 0000-0002-0616-030X

Notes

The authors declare no competing financial interest.

■ ACKNOWLEDGMENTS

This work was supported by the National Institutes of Health under Award No. DP2CA174508.

■ REFERENCES

(1) Tu, Y.; Peng, F.; Adawy, A.; Men, Y.; Abdelmohsen, L. K. E. A.; Wilson, D. A. Mimicking the Cell: Bio-Inspired Functions of Supramolecular Assemblies. *Chem. Rev.* **2016**, *116*, 2023−2078.

(2) Schwille, P. Bottom-Up Synthetic Biology: Engineering in a Tinkerer's World. *Science* **2011**, *333*, 1252−1254.

(3) Brea, R. J.; Rudd, A. K.; Devaraj, N. K. Nonenzymatic biomimetic remodeling of phospholipids in synthetic liposomes. *Proc. Natl. Acad. Sci. U. S. A.* **2016**, *113*, 8589−8594.

(4) Kurihara, K.; Okura, Y.; Matsuo, M.; Toyota, T.; Suzuki, K.; Sugawara, T. A recursive vesicle-based model protocell with a primitive model cell cycle. *Nat. Commun.* **2015**, *6*, 8352.

(5) Peng, F.; Tu, Y.; van Hest, J. C. M.; Wilson, D. A. Self-Guided Supramolecular Cargo-Loaded Nanomotors with Chemotactic Behavior towards Cells. *Angew. Chem., Int. Ed.* **2015**, *54*, 11662−11665.

(6) Yang, S.; Dai, X.; Stogin, B. B.; Wong, T.-S. Ultrasensitive surface-enhanced Raman scattering detection in common fluids. *Proc. Natl. Acad. Sci. U. S. A.* **2016**, *113*, 268−273.

(7) Pohorille, A.; Deamer, D. Artificial cells: prospects for biotechnology. *Trends Biotechnol.* **2002**, *20*, 123−128.

(8) Li, M.; Green, D. C.; Anderson, J. L. R.; Binks, B. P.; Mann, S. In vitro gene expression and enzyme catalysis in bio-inorganic protocells. *Chem. Sci.* **2011**, *2*, 1739−1745.

(9) Larsen, A. C.; Dunn, M. R.; Hatch, A.; Sau, S. P.; Youngbull, C.; Chaput, J. C. A general strategy for expanding polymerase function by droplet microfluidics. *Nat. Commun.* **2016**, *7*, 11235.

(10) Cheng, G.; Zheng, S.-Y. Construction of a high-performance magnetic enzyme nanosystem for rapid tryptic digestion. *Sci. Rep.* **2014**, *4*, 6947.

(11) Ghosh, P.; Yang, X.; Arvizo, R.; Zhu, Z.-J.; Agasti, S. S.; Mo, Z.; Rotello, V. M. Intracellular Delivery of a Membrane-Impermeable Enzyme in Active Form Using Functionalized Gold Nanoparticles. *J. Am. Chem. Soc.* **2010**, *132*, 2642−2645.

(12) Tang, R.; Kim, C. S.; Solfiell, D. J.; Rana, S.; Mout, R.; Velázquez-Delgado, E. M.; Chompoosor, A.; Jeong, Y.; Yan, B.; Zhu, Z.-J.; Kim, C.; Hardy, J. A.; Rotello, V. M. Direct Delivery of Functional Proteins and Enzymes to the Cytosol Using Nanoparticle-Stabilized Nanocapsules. *ACS Nano* **2013**, *7*, 6667−6673.

(13) Dewey, D. C.; Strulson, C. A.; Cacace, D. N.; Bevilacqua, P. C.; Keating, C. D. Bioreactor droplets from liposome-stabilized all-aqueous emulsions. *Nat. Commun.* **2014**, *5*, 4670.

(14) Shi, J.; Wang, X.; Zhang, W.; Jiang, Z.; Liang, Y.; Zhu, Y.; Zhang, C. Synergy of Pickering Emulsion and Sol-Gel Process for the Construction of an Efficient, Recyclable Enzyme Cascade System. *Adv. Funct. Mater.* **2013**, *23*, 1450−1458.

(15) Huang, X.; Appelhans, D.; Formanek, P.; Simon, F.; Voit, B. Tailored Synthesis of Intelligent Polymer Nanocapsules: An Investigation of Controlled Permeability and pH-Dependent Degradability. *ACS Nano* **2012**, *6*, 9718−9726.

(16) Parker, R. M.; Zhang, J.; Zheng, Y.; Coulston, R. J.; Smith, C. A.; Salmon, A. R.; Yu, Z.; Scherman, O. A.; Abell, C. Electrostatically Directed Self-Assembly of Ultrathin Supramolecular Polymer Microcapsules. *Adv. Funct. Mater.* **2015**, *25*, 4091−4100.

(17) Wong, C. K.; Laos, A. J.; Soeriyadi, A. H.; Wiedenmann, J.; Curmi, P. M. G.; Gooding, J. J.; Marquis, C. P.; Stenzel, M. H.; Thordarson, P. Polymersomes Prepared from Thermoresponsive Fluorescent Protein−Polymer Bioconjugates: Capture of and Report on Drug and Protein Payloads. *Angew. Chem., Int. Ed.* **2015**, *54*, 5317−5322.

(18) Huang, X.; Qian, K.; Yang, J.; Zhang, J.; Li, L.; Yu, C.; Zhao, D. Functional Nanoporous Graphene Foams with Controlled Pore Sizes. *Adv. Mater.* **2012**, *24*, 4419−4423.

(19) Fang, Y.; Zheng, G.; Yang, J.; Tang, H.; Zhang, Y.; Kong, B.; Lv, Y.; Xu, C.; Asiri, A. M.; Zi, J.; Zhang, F.; Zhao, D. Dual-Pore Mesoporous Carbon@Silica Composite Core−Shell Nanospheres for Multidrug Delivery. *Angew. Chem.* **2014**, *126*, 5470−5474.

(20) Liu, Y.; Goebl, J.; Yin, Y. Templated synthesis of nanostructured materials. *Chem. Soc. Rev.* **2013**, *42*, 2610−2653.

(21) Fang, X.; Liu, Z.; Hsieh, M.-F.; Chen, M.; Liu, P.; Chen, C.; Zheng, N. Hollow Mesoporous Aluminosilica Spheres with Perpendicular Pore Channels as Catalytic Nanoreactors. *ACS Nano* **2012**, *6*, 4434−4444.

(22) Li, M.; Harbron, R. L.; Weaver, J. V. M; Binks, B. P.; Mann, S. Electrostatically gated membrane permeability in inorganic protocells. *Nat. Chem.* **2013**, *5*, 529−536.

(23) Huang, X.; Li, M.; Green, D. C.; Williams, D. S.; Patil, A. J.; Mann, S. Interfacial assembly of protein−polymer nano-conjugates into stimulus-responsive biomimetic protocells. *Nat. Commun.* **2013**, *4*, 2239.

(24) Huang, Y.; Zhou, J.; Su, B.; Shi, L.; Wang, J.; Chen, S.; Wang, L.; Zi, J.; Song, Y.; Jiang, L. Colloidal Photonic Crystals with Narrow Stopbands Assembled from Low-Adhesive Superhydrophobic Substrates. *J. Am. Chem. Soc.* **2012**, *134*, 17053−17058.

(25) Vogel, N.; Utech, S.; England, G. T.; Shirman, T.; Phillips, K. R.; Koay, N.; Burgess, I. B.; Kolle, M.; Weitz, D. A.; Aizenberg, J. Color from hierarchy: Diverse optical properties of micron-sized spherical colloidal assemblies. *Proc. Natl. Acad. Sci. U. S. A.* **2015**, *112*, 10845−10850.

(26) Xu, X.; Tian, F.; Liu, X.; Parker, R. M.; Lan, Y.; Wu, Y.; Yu, Z.; Scherman, O. A.; Abell, C. Supracolloidal Architectures Self-Assembled in Microdroplets. *Chem. - Eur. J.* **2015**, *21*, 15516−15519.

DOI: 10.1021/acs.chemmater.6b04326
Chem. Mater. 2017, 29, 2081−2089

(27) Wilhelmina de Groot, G.; Demarche, S.; Santonicola, M. G.; Tiefenauer, L.; Vancso, G. J. Smart polymer brush nanostructures guide the self-assembly of pore-spanning lipid bilayers with integrated membrane proteins. *Nanoscale* **2014**, *6*, 2228−2237.
(28) Lu, Z.; Ye, M.; Li, N.; Zhong, W.; Yin, Y. Self-Assembled TiO_2 Nanocrystal Clusters for Selective Enrichment of Intact Phosphorylated Proteins. *Angew. Chem., Int. Ed.* **2010**, *49*, 1862−1866.
(29) Huang, Y.; Liu, M.; Wang, J.; Zhou, J.; Wang, L.; Song, Y.; Jiang, L. Controllable Underwater Oil-Adhesion-Interface Films Assembled from Nonspherical Particles. *Adv. Funct. Mater.* **2011**, *21*, 4436−4441.
(30) Yang, S.; Slotcavage, D.; Mai, J. D.; Liang, W.; Xie, Y.; Chen, Y.; Huang, T. J. Combining the Masking and Scaffolding Modalities of Colloidal Crystal Templates: Plasmonic Nanoparticle Arrays with Multiple Periodicities. *Chem. Mater.* **2014**, *26*, 6432−6438.
(31) Dinsmore, A. D.; Hsu, M. F.; Nikolaides, M. G.; Marquez, M.; Bausch, A. R.; Weitz, D. A. Colloidosomes: Selectively Permeable Capsules Composed of Colloidal Particles. *Science* **2002**, *298*, 1006−1009.
(32) Wu, C.; Bai, S.; Ansorge-Schumacher, M. B.; Wang, D. Nanoparticle Cages for Enzyme Catalysis in Organic Media. *Adv. Mater.* **2011**, *23*, 5694−5699.
(33) Liu, J.; Sun, Z.; Deng, Y.; Zou, Y.; Li, C.; Guo, X.; Xiong, L.; Gao, Y.; Li, F.; Zhao, D. Highly Water-Dispersible Biocompatible Magnetite Particles with Low Cytotoxicity Stabilized by Citrate Groups. *Angew. Chem., Int. Ed.* **2009**, *48*, 5875−5879.
(34) Cheng, G.; Zhang, J. L.; Liu, Y. L.; Sun, D. H.; Ni, J. Z. Synthesis of novel Fe_3O_4@SiO_2@CeO_2 microspheres with mesoporous shell for phosphopeptide capturing and labeling. *Chem. Commun.* **2011**, *47*, 5732−5734.
(35) Cheng, G.; Wang, Z.-G.; Denagamage, S.; Zheng, S.-Y. Graphene-Templated Synthesis of Magnetic Metal Organic Framework Nanocomposites for Selective Enrichment of Biomolecules. *ACS Appl. Mater. Interfaces* **2016**, *8*, 10234−10242.
(36) Tang, J.; Quinlan, P. J.; Tam, K. C. Stimuli-responsive Pickering emulsions: recent advances and potential applications. *Soft Matter* **2015**, *11*, 3512−3529.
(37) Yavuz, M. S.; Cheng, Y.; Chen, J.; Cobley, C. M.; Zhang, Q.; Rycenga, M.; Xie, J.; Kim, C.; Song, K. H.; Schwartz, A. G.; Wang, L. V.; Xia, Y. Gold nanocages covered by smart polymers for controlled release with near-infrared light. *Nat. Mater.* **2009**, *8*, 935−939.
(38) Ge, J.; Huynh, T.; Hu, Y.; Yin, Y. Hierarchical Magnetite/Silica Nanoassemblies as Magnetically Recoverable Catalyst−Supports. *Nano Lett.* **2008**, *8*, 931−934.
(39) You, Y.-Z.; Kalebaila, K. K.; Brock, S. L.; Oupický, D. Temperature-Controlled Uptake and Release in PNIPAM-Modified Porous Silica Nanoparticles. *Chem. Mater.* **2008**, *20*, 3354−3359.
(40) Chu, M.; Shao, Y.; Peng, J.; Dai, X.; Li, H.; Wu, Q.; Shi, D. Near-infrared laser light mediated cancer therapy by photothermal effect of Fe_3O_4 magnetic nanoparticles. *Biomaterials* **2013**, *34*, 4078−4088.
(41) Paul, A.; Laurila, T.; Vuorinen, V.; Divinski, S. V. *Fick's Laws of Diffusion*.; Springer: Berlin, Gemany, 2014.
(42) Doerr, A. Phosphorylation and the cell cycle. *Nat. Methods* **2008**, *5*, 858−859.
(43) Swami, M. Proteomics: A discovery strategy for novel cancer biomarkers. *Nat. Rev. Cancer* **2010**, *10*, 597.
(44) Ey, P.; Ferber, E. Calf thymus alkaline phosphatase. II. Interaction with detergents. *Biochim. Biophys. Acta* **1977**, *480*, 163−177.
(45) Smith, A. M.; Mancini, M. C.; Nie, S. Bioimaging: Second window for in vivo imaging. *Nat. Nanotechnol.* **2009**, *4*, 710−711.
(46) Zhang, Z.; Wang, Z.; Wang, F.; Ren, J.; Qu, X. Programmable Downregulation of Enzyme Activity Using a Fever and NIR-Responsive Molecularly Imprinted Nanocomposite. *Small* **2015**, *11*, 6172−6178.

DOI: 10.1021/acs.chemmater.6b04326
Chem. Mater. 2017, 29, 2081−2089